Deformation effects in the compound nucleus decay using the spin-alignment method

N. G. Nicolis, D. G. Sarantites, L. A. Adler, F. A. Dilmanian,* K. Honkanen,†
Z. Majka,‡ L. G. Sobotka, Z. Li,§ and T. M. Semkow**
Department of Chemistry, Washington University, St. Louis, Missouri 63130

J. R. Beene, M. L. Halbert, and D. C. Hensley
Oak Ridge National Laboratory, Oak Ridge, Tennessee 37830

J. B. Natowitz, R. P. Schmitt, D. Fabris,†† G. Nebbia,†† and G. Mouchaty
Cyclotron Institute and Department of Chemistry, Texas A&M University, College Station, Texas 77840
(Received 31 July 1989)

Alpha-particle energy spectra and angular distributions with respect to the estimated spin direction of residual nuclei have been measured in heavy-ion fusion reactions. The spin direction was determined for each event by measuring the γ-ray angular correlation patterns using the Spin Spectrometer. Measurements were made for the compound nuclear systems ^{110}Sn*(94 MeV), ^{114}Sn*(80 MeV), ^{138}Nd*(82 MeV), ^{164}Yb*(67 MeV), and ^{170}Yb*(135 MeV) at the indicated excitation energies as a function of the alpha-particle energy and γ-ray multiplicity. The anisotropy coefficients below the evaporation Coulomb barrier show distinct differences from ^{110}Sn* to ^{170}Yb*. These results and the shapes of the alpha-particle spectra are compared with statistical model calculations that incorporate deformation effects in the optical model transmission coefficients. The Sn* data can be explained without invoking deformation effects other than the ones included in the experimental yrast lines. However, for the heavier Yb* systems, a considerable spin-dependent deformation in the α-emission barriers is required. For these systems the α emission below the barrier is a sensitive probe for deformation that samples a broad range of excitation energies in the decay sequence.

I. INTRODUCTION

The study of nuclear shapes at high angular momentum and excitation energy is a topic of current extensive theoretical and experimental interest in heavy-ion physics. It is well known that collective nuclei near the yrast line are deformed, and their structure is well described by liquid-drop Strutinsky cranked shell model calculations. A question of interest is the evolution of these shapes as the spin and the excitation energy (temperature) are increased. There is already considerable experimental evidence for the existence of superdeformed nuclei ($\beta \approx 0.6$) at high spin.[1] Theoretical calculations that explain these highly deformed shapes predict even higher deformations ($\beta \approx 0.9$) for nuclei close to the fission stability limit.[2,3] Temperature-induced noncollective rotation in nuclei has been discussed with equilibrium shapes described by mean field theories, such as finite-temperature Hartree-Fock-Bogoliubov (HFB) cranking theory.[4] Increasing temperature at constant spin can induce phase transitions from one shape to another and from collective to noncollective rotation. Statistical shape fluctuations about the HFB shape have also been discussed.[5] A number of experimental studies have been designed to explore the effect of high excitation and/or angular momentum degrees of freedom on the nuclear shapes. These are made, on one hand, by exploiting the γ-decay properties (for example, study of giant resonances built on excited states) of the deexciting compound nuclei,[6,7] or on the other hand, by extensive searches to find signatures of shape effects in the charged-particle decay properties of excited systems.[8-13]

It is a well established fact that compound nuclei, with the highest possible angular momenta, often decay by emitting alpha particles.[14] Alpha-particle emission can therefore be used as a probe of nuclear shapes at very high spin, during the early stages of the deexcitation. Deformation effects make substantial changes in the transmission coefficients (T_l) for charged-particle emission, leading to strong enhancements of α decay, especially in the energy region below the evaporation Coulomb barrier.[8,9,15,16] Simulation studies along these lines have motivated a number of experiments consisting of the observation of alpha-particle spectra in heavy-ion fusion-evaporation reactions in a singles mode or in coincidence with evaporation residues.[9,13,16] The inability to reproduce the sub-barrier part of the observed alpha spectra with statistical model calculations assuming spherical emission shapes has indicated the need to introduce new effects in the statistical model (see Ref. 43 and references therein). Deformation effects have been discussed in this context in Refs. 9-13.

Besides the interesting problem of selecting the proper parameter set for calculating the T_l's (Refs. 8, 15, and 17) and therefore interpreting such data on solid ground, one has to consider the following facts: (a) the correlation of interest is that between the α-emission direction and the spin direction (which in the case of fusion of spinless nuclei, is uniformly distributed on a plane perpendicular to the beam axis), and (b) the α-decay competition is nor-

mally expected to vary with the compound nucleus angular momentum.

The above facts led us to the development of the spin alignment method with the 4π γ-ray Spin Spectrometer.[18,19] In this method, the magnitude and orientation of the spin of the residual nuclei are deduced on an event-by-event basis. This makes possible detailed studies, such as the measurement of alpha-particle angular distributions with respect to the estimated spin direction.[20] Furthermore, the γ-multiplicity selection with the Spin Spectrometer allows us to study these decay characteristics as a function of the evaporation residue spin, which is closely correlated with the compound nucleus spin. Therefore, the α-decay properties of different compound nuclear systems can be studied in detail.[10-12]

In this paper, alpha-particle energy spectra and angular distributions with respect to the estimated spin direction are reported for a number of compound nuclear systems ranging from the closed shell ^{110}Sn* to the rare earth ^{170}Yb*. The α-emission properties of these systems are described by the anisotropy coefficients of the alpha-particle emission with respect to the estimated spin direction as a function of the alpha-particle energy and γ-ray multiplicity. Differences in the emission patterns, in the energy region below the evaporation Coulomb barrier, suggest a nearly spherical shape in the case of ^{110}Sn* and a deformed emission shape for ^{170}Yb*. Further evidence of these effects is found in the behavior of the 90° center of mass spectra, when proper γ-multiplicity gates are imposed. As discussed in Sec. IV E, these findings are corroborated by both the known ground-state properties and data of giant resonances built on excited states of similar compound nuclear systems. The data for ^{138}Nd* and ^{164}Yb* show a progressively increasing deformation effect, intermediate to that observed for ^{110}Sn* and ^{170}Yb*. Detailed statistical model calculations have been performed to clarify the deviations of the "deformed" versus the "spherical" behavior. In the sub-barrier region, the predictions of the statistical model for charged-particle emission are sensitive to barrier penetration effects. These effects are expressed in terms of transmission coefficients resulting from an optical model calculation. Different optical model parameter sets were employed to investigate the behavior of the 90° center of mass (c.m.) spectra and anisotropy coefficients in the emission with respect to the estimated spin direction. Selecting as a reference spherically symmetric set the one which closely describes the decay of the Sn* isotopes, we observe discrepancies for the other systems. These discrepancies become more apparent in the Yb* isotopes and appear as (a) underestimates of the sub-barrier contribution to the 90° c.m. spectra; (b) underestimates of the multiplicity-gated 90° c.m. spectra, which increase with spin; and (c) deviations in the trend of the anisotropy coefficients from the one predicted in the Sn* case, which also increase with spin. With a simple model, we show that inclusion of deformation effects in the transmission coefficients for charged-particle emission provides a good description of the alpha-particle spectra. A detailed comparison with the ^{170}Yb* data is made, which shows the angular momentum dependence of the deformation effect in the alpha spectra. However, more elaborate calculations are required to describe the corresponding effect in the anisotropy coefficients of these systems. Despite these successes, the utility of the alpha-particle emission for studying nuclear shapes at high E^* is hampered by the broad range of initial excitation energies which contribute in low-energy particle emission.

The structure of this paper is the following. Sections II and III contain the experimental methods and the results concerning the alpha-particle spectra and anisotropy coefficients for all of the systems under study. The experimental data are compared with the predictions of the statistical model with standard parameters in Secs. IV A–IV C. A simulation of deformation effects in the transmission coefficients and its implications are given in Secs. IV D and IV E. Finally Sec. V contains the conclusions of this research.

II. EXPERIMENTAL METHODS

The experiments in this work were performed at the Oak Ridge Holifield Heavy-Ion Research Facility (HHIRF). The compound systems studied[12] were ^{114}Sn*, ^{138}Nd*, and ^{164}Yb*. This completes earlier published studies[10,11] involving the compound nuclei ^{110}Sn* and ^{170}Yb*. A summary of the reactions used to produce the above compound systems and bombarding conditions are given in Table I.

Self-supporting targets of high isotopic enrichment

TABLE I. Summary of reaction parameters of the compound systems studied.

Reaction	E_L[a] (MeV)	Target thickness (μg/cm^2)	E^*[a] (MeV)	$E_{c.m.}/V_b$[b]	l_{cr}[c] ($\hbar$)
^{45}Sc+^{65}Cu→^{110}Sn*	200.0	320–450	93.9	1.41	70.1
^{64}Ni+^{50}Ti→^{114}Sn*	250.0	500	79.5	1.30	65.3
^{64}Ni+^{74}Ge→^{138}Nd*	270.0	760	82.4	1.25	79.1
^{64}Ni+^{100}Mo→^{164}Yb*	270.0	990	67.2	1.14	73.6
^{20}Ne+^{150}Nd→^{170}Yb*	176.6	1100	134.8	2.01	76.6

[a] E_L and E^*: beam and initial excitation energy in the middle of the target.

[b] $E_{c.m.}/V_b$: ratio of the center of mass energy to the entrance channel Coulomb barrier estimated as $V_b = e^2 Z_1 Z_2 / r_0 (A_1^{1/3} + A_2^{1/3})$, where $r_0 = 1.4$ fm.

[c] l_{cr}: critical angular momentum for fusion corresponding to $\sigma_{fus} = \pi \lambda^2 \sum (2l+1) T_l$, where $T_l = \{1 + \exp[(l - l_{cr})/\Delta]\}^{-1}$ and $\Delta = 2\hbar$. Here σ_{fus} was calculated with the Bass model (see Table II).

were used in all cases (see Table I). In the experiments employing ^{64}Ni beams, the alpha particles were detected with four Si surface barrier telescopes positioned at the laboratory angles 60°, 65°, 60° and 60°. The locations of these telescopes were selected to correspond to ~90° in the center of mass system for the ^{114}Sn*, ^{138}Nd*, and ^{164}Yb* systems. A similar arrangement was used in the earlier experiments (^{170}Yb* and ^{110}Sn*), where the alpha particles were also detected near 90° in the center of mass.[10,11] These detectors provide complete information, in connection with the spin-alignment method, because they sample the entire $W(\beta)$ distribution of emitted alpha particles with respect to the estimated spin direction($0° \leq \beta \leq 90°$). The 90° ΔE detectors had a thickness of ~25 μm and an acceptance cone of ~6° half angle. The corresponding E detectors were 1500 μm thick and served as the triggers of the Spin Spectrometer. The Spin Spectrometer served as the γ-ray detector and measured simultaneously the γ-ray multiplicity M_γ, the total γ-ray deexcitation energy, and the γ-ray angular correlations. In these experiments 71 out of the 72 detectors of the Spin Spectrometer were used. The solid angle covered was 95.8% of 4π sr.

The utility of the Spin Spectrometer to select rather narrow regions of spin in order to study decay patterns has been discussed earlier.[12,19] Since the α-emission patterns vary smoothly with spin, selection of somewhat broad spin regions corresponding to coincidence fold intervals of $\Delta k_\gamma = 3$ or 4 is sufficient in these studies and helps to improve the statistics. A typical distribution of γ-ray coincidence fold (k_γ) for events triggered by alpha particles (detected at 90° in c.m.) from the decay of the ^{110}Sn* compound system is shown in Fig. 1(a). This distribution is closely related to the M_γ distribution and indicates that the spin distribution extends to high angular momenta for this system. The small bump at $k_\gamma \approx 8$ is due to sequential emission from fissionlike decay channels.[21] Such bumps in the multiplicity distribution have been observed in the decay of even more fissile systems with compound nucleus mass up to $A \approx 170$. These channels transfer a substantial fraction of the available angular momentum into an orbital component and therefore are associated with low M_γ or k_γ. The data shown in Sec. III are based on events sorted for $k_\gamma \geq 9$ for ^{110}Sn* and $k_\gamma \geq 11$ for the other systems. The spill over of fissionlike events into the first k_γ bin is estimated to be <3% for the Sn* systems, <5% for ^{138}Nd*, and ~20–25 % for the Yb* systems. All of the other k_γ bins are essentially free of fission contributions.

The method used for determining the spin direction is based on the angular distribution of γ radiation with a particular angular relationship to the spin direction.[20] The γ cascades from rotational nuclei formed in heavy-ion fusion-evaporation reactions have a preponderance of stretched $E2$ transitions ($\Delta I = 2, L = 2, M = 2$) which exhibit a toroidal pattern about the spin axis [$W(\theta) = \frac{5}{4}(1 - \cos^4\theta)$]. This pattern is enhanced by the presence of nonstretched dipole transitions ($\Delta I = 0, L = 1, M = 0$) [$W(\theta) = \frac{3}{2}(1 - \cos^2\theta)$], while the presence of stretched dipoles ($\Delta I = -1, L = 1, M = 1$) [$W(\theta) = \frac{3}{4}(1 + \cos^2\theta)$] has the effect of filling the hole of the toroid.[20] The spin direction is identified with the short symmetry axis of this pattern. This is close to the compound nucleus spin, i.e., perpendicular to the beam, provided that the misalignment caused by particle emission is small. This assumption improves at high spin, where stretched particle emission dominates. In the off-line analysis, the γ pattern for each event was projected on a plane perpendicular to the beam direction and centroid-searching methods were used to determine the angle between the short symmetry axis and the direction of the emitted alpha particle. The use of the γ-radiation patterns in determining the spin direction can be tested by examining the α-γ angular correlations. In Fig. 1(b) we show the angular distribution of γ rays in the plane perpendicular to the beam direction from the decay of ^{110}Sn*. Here the alpha particles were detected at an azimuthal angle $\phi = 150°$ and k_γ was between 14 and 23. This pattern is indeed consistent with a preponderance of stretched $E2$ and/or nonstretched dipole transitions and justifies the use of the spin-alignment technique for estimating the spin direction.[20]

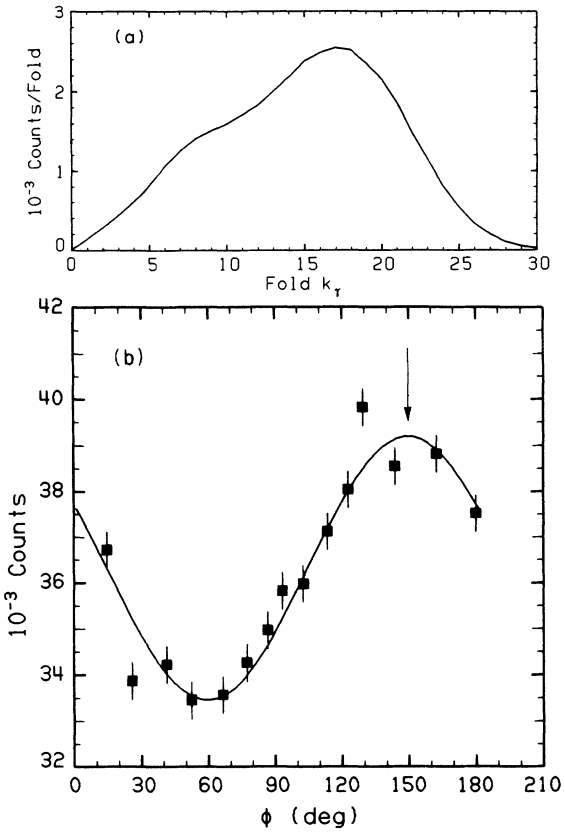

FIG. 1. (a) Distribution of the γ-ray coincidence fold k_γ for events triggered by alpha particles detected near $\theta_{c.m.} = 90°$ from 200 MeV ^{45}Sc on ^{65}Cu. (b) Angular distribution of the γ rays emitted in the plane perpendicular to the beam from events with an alpha particle emitted at $\phi = 150°$ (vertical arrow). The pattern is consistent with a preponderance of stretched $E2$ transitions. The solid curve is a least-squares fit to $A_0[1 + A_2 P_2(\cos\phi)]$.

The factors that determine the spin orientation event by event from Spin Spectrometer data have been outlined in detail in our earlier work.[10] The two most important factors which influence the spin-alignment response functions are the γ-ray multiplicity and the multipolarities present in the ensemble of γ cascades.[20] The former is easily accounted for by simulations,[20] while the latter may play an important role when different nuclear systems are compared.

III. EXPERIMENTAL RESULTS

For each compound nuclear system (A_{CN},Z_{CN}), the alpha-particle events were transformed to the center of mass system for $\alpha+(A_{CN}-4,Z_{CN}-2)$, using two-body kinematics. The evaporation of several neutrons prior to α emission has been found to have a negligible effect on the center of mass energy and angle.[10] In the following analysis, alpha-particle events corresponding to emission angles near $\theta_{c.m.}=90°$ were sorted, for all of the systems, imposing different γ-coincidence fold (k_γ) gates, or gates on the alpha-particle emission angle (β) with respect to the estimated spin direction.

The experimental 90° center of mass spectra integrated over k_γ and β are discussed in Sec. IV, where they are compared with statistical model calculations. However, some useful remarks can be made from an inspection of multiplicity-decomposed spectra. Figure 2(a) shows the 90° center of mass spectra for the decay of the ^{110}Sn* system, corresponding to the four $k_\gamma=9-13$, 14–18, 19–23, and 24–30 gates, represented by squares, circles, triangles, and diamonds, respectively. The shape of these evaporative spectra does not change significantly with fold. However, a close inspection reveals that the low-multiplicity-gated spectrum ($k_\gamma=9-13$) has a small excess of sub-barrier alphas compared to the high-multiplicity ($k_\gamma=24-30$) spectrum. This trend seems to be amplified in the case of ^{114}Sn*, shown in Fig. 2(b). The spectra corresponding to $k_\gamma=11-14$ and $k_\gamma=27-33$ are represented by squares and circles, respectively. Here, the low-fold spectrum shows a shift in its peak position to lower energy. At the same time, it appears to be harder than the $k_\gamma=27-33$ spectrum. Qualitatively, the difference in the slopes can be understood by the fact that the low-fold gate selects states of higher intrinsic excitation energy. Therefore, the corresponding particle spectra show a higher temperature. The fact that ^{110}Sn* does not show such slope changes is attributed to multiple alpha emission in this more neutron-deficient isotope. The above trends are discussed in connection with statistical model calculations in Sec. IV B. The above situation is reversed in the case of ^{170}Yb*, as far as the sub-barrier behavior is concerned. In Fig. 2(c), we show the 90° center of mass spectra produced with the same gates $k_\gamma=11-14$ (squares) and $k_\gamma=27-33$ (circles). The low-k_γ spectrum is harder, but the high-k_γ spectrum now has slightly more sub-barrier alphas. A similar trend has been observed in the other systems: ^{138}Nd* and ^{164}Yb*. Such a behavior is opposite to the one predicted by the statistical model assuming spherical emitters, as explained in Sec. IV B.

The ability to determine the spin direction event by event allows the observation of other interesting correlations in the observed spectra. One can study, for example, the spectra corresponding to different alpha-particle emission angles (β) with respect to the estimated spin direction, in a particular γ-coincidence fold gate. This is demonstrated in Fig. 3, where alpha energy spectra corresponding to a low and a high k_γ-gate, at angles almost parallel (9°–11°) and perpendicular to the estimated spin

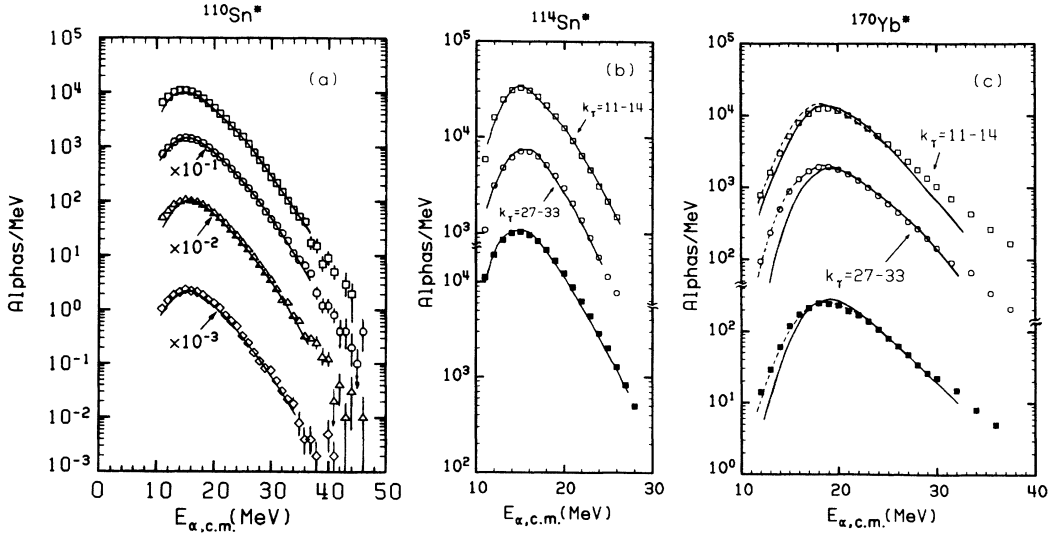

FIG. 2. (a) Spectra of alpha particles observed at $\theta_{c.m.}=90°$ from the ^{110}Sn* system corresponding to the bins: squares, circles, triangles, and diamonds are for $k_\gamma=9-13$, 14–18, 19–23, and 24–30, respectively. (b) γ-fold gated 90° center of mass alpha-particle spectra from ^{114}Sn*. The squares correspond to $k_\gamma=11-14$ and the circles to $k_\gamma=27-33$. (c) γ-fold gated 90° center of mass alpha-particle spectra from ^{170}Yb*. The squares correspond to $k_\gamma=11-14$ and the circles to $k_\gamma=27-33$. In (b) and (c), the closed squares represent the total ($k_\gamma=11-33$) spectra. The solid and dashed lines are the results of statistical model calculations described in the text.

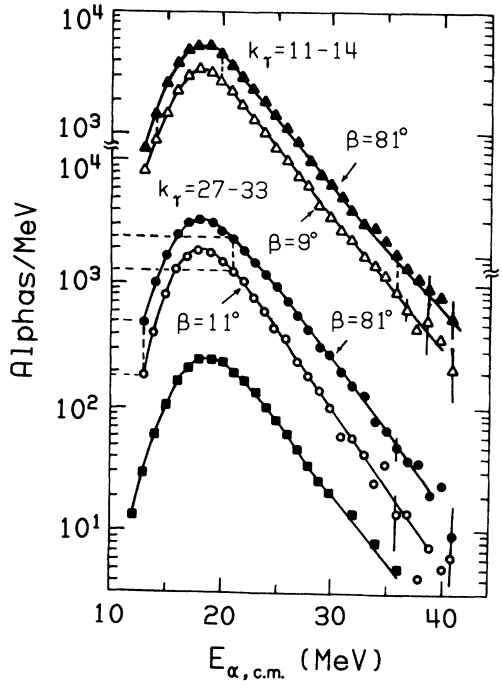

FIG. 3. Alpha-particle spectra from ^{170}Yb*. Top: Spectra corresponding to $k_\gamma=11-14$, $\beta=9°$ (open triangles) and 81° (solid triangles). Middle: Spectra corresponding to $k_\gamma=23-26$, $\beta=11°$ (open circles) and $\beta=81°$ (solid circles) with respect to the estimated spin direction. The experimental spectrum integrated over k_γ and β is shown in the lower part by the solid squares. The solid lines guide the eye.

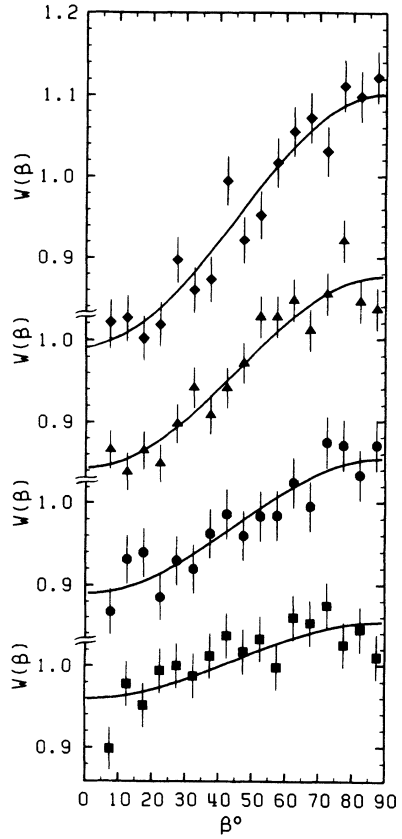

FIG. 4. Experimental angular correlations of alpha particles with respect to the estimated spin direction of the residual nucleus ^{110}Sn*. The triangles and diamonds correspond to $E_\alpha=13$ MeV for the k_γ gates of 14–18 and 19–23, respectively. The squares and circles correspond to the k_γ gate of 9–13 for $E_\alpha=13$ MeV and 20 MeV, respectively. The solid lines are least-squares fits of $A_0[1+A_2P_2(\cos\beta)]$ to the data.

direction (81°) are plotted and compared to the total center of mass spectrum of ^{170}Yb*. The spin angle labels represent the centroids of the estimated spin direction for selected 18° wide β-angle bins. On the top, the open and solid triangles correspond to a $k_\gamma=11-14$ gate and $\beta=9°$ and 81°. In the middle, the open and solid circles correspond to a $k_\gamma=23-26$ gate and $\beta=11°$ and 81°, respectively. The total spectrum, integrated over k_γ and β, is shown in the lower part of the figure, for comparison. The spectra have been shifted along the vertical axis for display purposes, and the solid lines guide the eye. The $\beta=11°$ and $\beta=9°$ spectra are similar, except for a difference in their high-energy slopes, the $k_\gamma=11-14$ gated one being harder. However, in each k_γ fold, one observes differences with the spectra corresponding to the emission perpendicular to the estimated spin direction, both above and below the Coulomb barrier. These differences are depicted by dashed horizontal and vertical lines and give us a measure of the anisotropies of the α emission with respect to the estimated spin direction. These differences become stronger when k_γ increases from 11–14 to 23–26.

An efficient way of examining these differences in the decay properties of these systems is to construct the angular correlation between the estimated spin direction and the direction of emission of alpha particles of a given center of mass energy, as a function of the γ multiplicity. Examples of such angular correlations from the ^{110}Sn* system are shown in Fig. 4 for a given k_γ gate of (9–13) and two α energies of 13 and 20 MeV (squares and circles) and for a given α energy of 13 MeV and two k_γ gates of 14–18 and 19–23 (triangles and diamonds, respectively). We see that for a given $E_\alpha=13$ MeV the anisotropy of the correlation increases as k_γ is increased, indicating a favoring of α emission perpendicular to the spin direction. We also observe that, for a given k_γ gate, the emission perpendicular to the spin direction also increases with increasing E_α. The dependence of the measured correlations on E_α can be best demonstrated by fitting the correlations to the function

$$W(\beta)=A_0[1+A_2P_2(\cos\beta)+A_4P_4(\cos\beta)]$$

for all of the systems. Examples of fits with the above expression are shown by the solid lines in Fig. 4. A negative A_2 value indicates that $W(\beta=90°)/W(\beta=0°)>1$. The A_4 coefficients have, in general, been found to be small and essentially independent of E_α. We therefore report the A_2 coefficients as a function of E_α.

The extracted A_2 coefficients are plotted versus E_α in

Figs. 5(a)–(e) for various k_γ gates, as indicated, for the ^{110}Sn*, ^{114}Sn*, ^{138}Nd*, ^{164}Yb*, and ^{170}Yb* systems, respectively. The Coulomb barriers for α emission from the corresponding compound nuclei are indicated by vertical arrows for each system. They were estimated assuming touching spherical nuclei and a radius parameter $r_0 = 1.4$ fm. The pairs of curves are FWHM boundaries of the A_2 coefficients from a statistical model calculation described in the next section. Certain trends are observed in the experimental data. For each of the systems studied, for a given E_α, the A_2 values become monotonically more negative as the coincidence fold k_γ is increased. The dependence of A_2 on E_α, however, exhibits patterns characteristic of each system under study. First of all, there is a similarity in the decay patterns of ^{110}Sn* and ^{114}Sn* [Figs. 5(a) and (b)]. The A_2 coefficients become monotonically more negative (larger anisotropies) as E_α is increased from values well below the barrier to the highest energies of the measurements. However, the A_2 coefficients of ^{110}Sn* have a smaller absolute value. In contrast with these findings, the A_2 coefficients for ^{170}Yb*, Fig. 5(e), have an absolute maximum at the Coulomb barrier ($\approx$20 MeV) and become more negative at both lower and higher E_α values. Compared with the almost linear decrease with E_α of the Sn*'s, we see a deviation in the trend of the experimental correlations below the Coulomb barrier. The ^{170}Yb data show much larger anisotropies, increasing with γ-coincidence fold.

Qualitatively, the trend of the A_2 coefficients for ^{110}Sn*, ^{114}Sn* as a function of E_α can be understood in the following terms. The α angular distribution is determined by the combined effect of the transmission

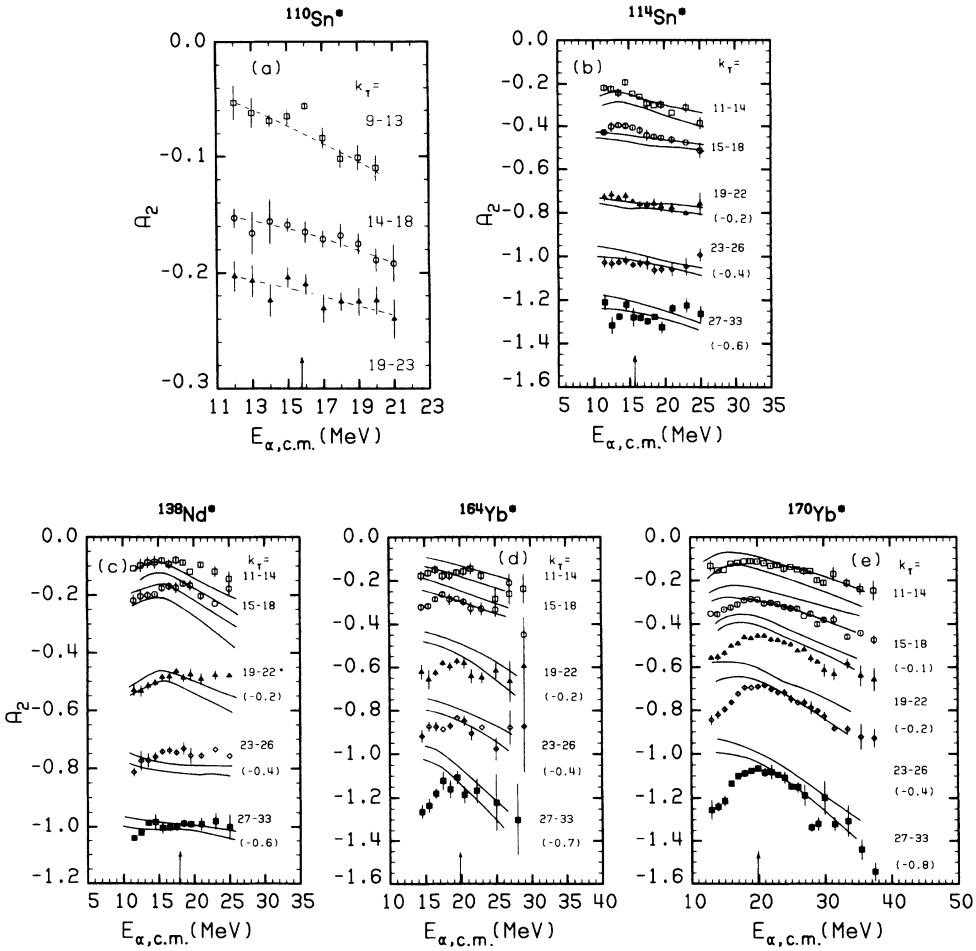

FIG. 5. A_2 coefficients as a function of $E_{\alpha,\mathrm{c.m.}}$ from the five systems studied. The vertical arrows indicate the position of the spherical Coulomb barrier calculated with $r_0 = 1.4$ fm. (a) Results from ^{110}Sn* decay. The squares, circles, and triangles are for k_γ bins of 9–13, 14–18, and 19–23, respectively. The dashed lines guide the eye. In (b), (c), and (d) the results for ^{114}Sn*, ^{138}Nd*, and ^{164}Yb* are shown; the open squares, circles, solid triangles, diamonds, and solid squares correspond to the k_γ bins of 11–14, 15–18, 19–22, 23–26, and 27–33, respectively. In some cases the data have been shifted along the A_2 axis by the indicated amount. (e) Results from ^{170}Yb decay. From top to bottom, the solid circles, open circles, triangles, large solid circles, and solid squares correspond to k_γ bins of 11–14, 15–18, 19–22, 23–26, and 27–32 ($I \approx 34\hbar$, $43\hbar$, $51\hbar$, $59\hbar$, and $64\hbar$), respectively. The pairs of curves are FWHM boundaries of the A_2 coefficients from a statistical model calculation using transmission coefficients from a spherical optical model potential.

coefficients for α decay $T_l(E_\alpha)$ and the level density. For a given E_α, T_l is constant up to some l and then decreases monotonically. The level density favors transitions with large ΔI. As E_α increases, the T_l's for larger l increase, leading to monotonically increasing anisotropies. On the other hand, for a spherical emitting nucleus and energies below the Coulomb barrier, the number of effective l waves with $T_l \neq 0$ diminishes rapidly with decreasing E_α, leading eventually to isotropy. Therefore, the decay patterns of the Sn* isotopes are indicative of nearly spherical emitting systems.

The deviation of the ^{170}Yb* data from the above trend occurs at low emission energies which are sensitive to details of the Coulomb barrier. It has been suggested that nuclear deformation is responsible for the decrease of the measured A_2 coefficients at low E_α.[10] If the emitting system is deformed with its longest axis perpendicular to the spin direction, the sub-barrier alpha particles will be emitted preferentially along this direction (because of the lower Coulomb barrier). This leads to decreasing A_2 coefficients with decreasing E_α, i.e., enhanced anisotropies. On the other hand, the trend of the A_2 coefficients above the barrier would not be affected much by details in transmission, because the emission is mainly determined by the level densities. Therefore, the observed deviations indicate the existence of a deformation effect which increases with spin.

Comparing the behavior of the experimental A_2 coefficients for the other systems of Fig. 5, we observe deviations of intermediate magnitude. A mild deformation effect is suggested by the decay of ^{138}Nd*. A stronger deformation, comparable to the one observed in its neighboring ^{170}Yb* system, is implied by the ^{164}Yb* data.

IV. STATISTICAL MODEL CALCULATIONS

A. Parameters

For a quantitative description of the observed effects, detailed statistical model calculations were performed. A direct comparison between theory and our experimental data necessitates the use of Monte Carlo techniques. With this method, we obtain a comparison between the experimental data and the theoretical predictions under the restrictions imposed by our gating conditions.

In the following analysis, we made use of a modified version of the code PACE2S (Ref. 22), called hereafter PACE2D. This version allows a more complete treatment of the optical model transmission coefficients (T_l) for charged-particle emission. Instead of the previously used extrapolation procedure,[22] complete optical model calculations were performed for proton and α emission. Calculations were performed for isotopes in 20×10 (N,Z) grids which span the range of isotopes considered in each statistical model calculation. Energy ranges of 3–33 MeV for protons and 5–35 MeV for alpha particles were considered in steps of 1 MeV. Such sets of T_l for each energy and type of emitted particle were stored in computer files to be read by PACE2D. Transmission coefficients for nonintegral energy values were calculated by logarithmic interpolation. For neutrons, the internal calculation employed by PACE2S was retained.

In the optical model calculations, the parameters of Wilmore and Hodgson[23] and Perey and Perey[24] were used for neutrons and protons, respectively. Various optical model parametrizations for alpha particles were tested,[25,26] besides the one used in the old version of the code.[22] In the calculation we describe below, we used the optical model parameters given by McFadden and Satchler.[25] This selection was based on (a) an overall better agreement they provide in the description of the sub-barrier part of the α spectrum and A_2 coefficients for the Sn* systems and (b) the fact that they provide a close description of fusion data on targets with mass close to our compound nuclei in the Yb mass region, as discussed in Sec. IV E.

Statistical model calculations were performed for all of the reaction systems under study. The relevant parameters are summarized in Table II. The compound nucleus angular momentum distributions were assumed to be of the form

$$\sigma_l = \pi\lambda^2(2l+1)\{1+\exp[(l-l_{\rm cr})/\Delta]\}^{-1} ,$$

where the critical angular momentum for fusion $l_{\rm cr}$ was determined by the requirement that $\sum\sigma_l$ reproduces the fusion cross section $\sigma_{\rm fus}$ with an assumed diffuseness parameter $\Delta = 2\hbar$. Here, $\sigma_{\rm fus}$ was taken from the prediction of the Bass model,[27] except for the reaction ^{20}Ne+^{150}Nd, where the experimentally measured fusion cross section[28] was used. The level densities were calculated with Fermi gas level density expression,[22] and the parameters listed in Table II. The code normally employs yrast lines taken from the rotating diffuse liquid-drop model calculation with finite-range corrections of Sierk.[29] However, it was found that these yrast lines, at each spin, are lower than the experimental ones, which in most of the cases are known up to spin $\approx 30\hbar$.[30] For this reason, all of the liquid-drop yrast lines $E_{{\rm rot},I}$ were given a linear shift up to spin $I = 24\hbar$. A constant shift $\Delta E_{\rm yr}$ was added for $I \geq 24\hbar$:

$$E_{{\rm rot},I} \rightarrow \Delta E_{\rm yr} \times \frac{I}{24} + E_{{\rm rot},I}, \quad I < 24\hbar$$

$$\rightarrow \Delta E_{\rm yr} + E_{{\rm rot},I}, \quad I \geq 24\hbar .$$

In addition, the odd mass yrast lines were shifted up in spin by $\Delta I_{\rm yr} = \Delta I \times (1 - I/40)$ for $I \leq 40\hbar$. Such a modification with the $\Delta E_{\rm yr}$ and $\Delta I_{\rm yr}$ values of Table II gives good agreement with existing yrast level schemes for nuclei involved in our reactions. The liquid-drop yrast lines[29] were used as an extrapolation of the experimental values according to the above scheme.

The $E1$ γ-ray emission strength function included the giant dipole resonance (GDR) with shape and position taken from systematics[31,32] and strength determined by the energy weighted sum rule.[31] GDR splittings due to deformation were included using a double Lorentzian GDR shape corresponding to a deformation $\beta_{\rm GDR}$. Statistical $E1$ and $M1$ transitions as well as collective

TABLE II. Reaction parameters pertaining to the statistical model calculations for the reaction systems under study.

Quantity	^{64}Ni+^{50}Ti $\rightarrow ^{114}$Sn*	^{64}Ni+^{74}Ge $\rightarrow ^{138}$Nd*	^{64}Ni+^{100}Mo $\rightarrow ^{164}$Yb*	^{20}Ne+^{150}Nd $\rightarrow ^{170}$Yb*
E_L (MeV)	250	270	270	176.6
E^* (MeV)	79.5	82.4	67.2	134.8
σ_{fus} (mb)	943.25	860.49	579.86	1548.94
B_f (MeV)	38.4	32.3	23.4	25.1
σ_{fiss} (mb)	23.4	219.9	167.6	280.4
a (MeV^{-1})	$A/9.0$	$A/6.5$	$A/8.5$	$A/9.5$
$B(E1)$ (W.u.)	1.0	1.0	1.0	1.0
$B(M1)$ (W.u.)	0.007	0.007	0.05	0.05
$B(E2)_{stat}$ (W.u.)	5.0	6.0	10.0	10.0
$B(E2)_{coll}$ (W.u.)	50	60	60	60
$B(M2)$ (W.u.)	0.05	0.058	0.000 88	0.000 88
ΔE_{yr} (MeV)	3.5	2.5	2.0	2.0
ΔI_{yr} (MeV)	4.0	3.0	8.0	8.0
β_{GDR}	0.1	0.2	0.3	0.3

stretched $E2$ transitions for $E_\gamma \leq 2$ MeV were included with the strengths of $B(E2)$, $B(M1)$, and $B(E2)_{coll}$ of Table II.

Fission barriers were the Sierk diffuse-surface liquid-drop barriers.[29] The ratio of the single-particle level density of the nucleus at the saddle-point deformation to that at equilibrium deformation was taken as $a_f/a_\nu = 1$.

The objective of the calculations was to investigate the 90° center of mass spectra and the observed trend of the anisotropy coefficients A_2. Care was taken so that the optical model and statistical model parameters used for ^{170}Yb* (see Table II) closely reproduce the measured xn and αxn evaporation residue cross sections.[33] For the other systems there are no xn or αxn cross section data available.

B. The alpha-particle spectra

Event files from PACE2D were sorted to obtain the alpha-particle spectra at 90°±5° in the center of mass system corresponding to evaporation residues with γ multiplicity $M_\gamma \geq 11$. The calculated spectra for the decay of the compound systems ^{114}Sn*, ^{138}Nd*, ^{164}Yb*, and ^{170}Yb* are shown in Figs. 6(a)–(d) by dashed lines. They have been normalized to the total number of counts in the experimental spectra, except for the case of ^{164}Yb*, where a normalization for energies higher than the peak position was applied. The ^{114}Sn* spectrum is reproduced in shape and maximum position. There is a small overestimate of the α yield around the maximum. The maximum of the α spectrum from ^{138}Nd* is also predicted at a slightly higher energy, and the low-energy part is slightly underpredicted. The ^{164}Yb* and ^{170}Yb* spectra are also underpredicted in the sub-barrier region, the discrepancies being much greater, although the high-energy slopes are reproduced. In both cases, the calculated spectra peak at a higher energy. For ^{170}Yb*, the underprediction of the spectrum at high energies (> 30 MeV) is associated with a small nonequilibrium component.[10]

The γ-fold gated spectra at 90° center of mass are compared with the theoretical predictions in Fig. 2. It has to be remembered that these spectra still contain an integration of the spin direction about the beam direction, for each fold. In Fig. 2(a), the solid lines show the calculated spectra corresponding to the different k_γ bins, for ^{110}Sn*. In all cases, the peak positions and high-energy slopes are well reproduced. Similarly, good agreement is obtained for the ^{114}Sn* for the two k_γ-gated spectra, as shown by the solid lines in Fig. 2(b). In the case of ^{170}Yb*, we have large discrepancies, as shown in Fig. 2(c). The calculation described above corresponds to the solid lines. The $k_\gamma = 11-14$ spectrum is underpredicted in the sub-barrier region. There is also a discrepancy in the description of the high-energy tail. In the (high) $k_\gamma = 27-33$ gate, the discrepancy is only in the sub-barrier region, and is much larger. The general features of the statistical model calculation of the multiplicity-gated spectra of Fig. 2 are the following: The behavior of the ^{110,114}Sn* spectra is well reproduced. For ^{170}Yb*, the sub-barrier parts of the spectra are underpredicted, and this increases with spin. As will be shown in Sec. IV D, these discrepancies tend to disappear when the calculations are taking into account the nonsphericity of nuclei in the treatment of the transmission coefficients.

The above calculations show that in the reactions under study, there is only one alpha particle emitted in more than ≈94% of the cascades involving α emission. The deexcitation of ^{110}Sn* is the only exception, where the α multiplicity distribution, for α folds of 1, 2, and 3, is predicted to be 48%, 38%, and 12%, respectively.

C. The A_2 coefficients

The alpha-particle angular distribution $W_{E_\alpha, I_i, I_f}(\beta)$ for an initial spin I_i and final spin I_f relative to the spin direction can be expressed as a Legendre polynomial expansion:[10]

$$W_{E_\alpha, I_i, I_f}(\beta) = \sum_\lambda a_{E_\alpha, I_i, I_f, \lambda} B_\lambda(I_i) P_\lambda(\cos\beta) , \quad (1)$$

where

$$a_{E_\alpha,I_i,I_f,\lambda}=\sum_l \frac{T_l(E_\alpha)}{\sum_{l'}T_{l'}(E_\alpha)}(-1)^{I_i+I_f}(2l+1)(2I_i+1)^{1/2}(2\lambda+1)^{1/2}\begin{bmatrix} l & l & \lambda \\ 0 & 0 & 0 \end{bmatrix}\begin{Bmatrix} l & l & \lambda \\ I_i & I_i & I_f \end{Bmatrix}. \quad (2)$$

The coefficients of the expansion appear as a product of the theoretical anisotropies $a_{E_\alpha,I_i,I_f,\lambda}$ and the attenuation coefficients $B_\lambda(I_i)$. The experimental A_2 coefficients correspond to $\sum_i a_{E_\alpha,I_i,I_f,2}B_2(I_i)$, where the summation runs over the initial spins I_i, for a given E_α and M_γ. The $T_l(E_\alpha)$, in Eq. (2), are transmission coefficients associated with the emission of an alpha particle of energy E_α and angular momentum l.

The $B_\lambda(I_i)$ are the statistical tensors describing the ensemble of spin orientations with respect to the quantization axis. They are derived from the spin-alignment responses of the spin spectrometer using the vector model.[10,20] The spin-alignment responses, for a given γ multiplicity M_γ and multipolarity mixture of the emitted γ rays were parametrized with three terms C_1, C_2, and σ_β in a relation of the form

$$P(\beta,M_\gamma)=C_1+C_2\exp\left[-\frac{(\beta-90°)^2}{2\sigma_\beta^2}\right]. \quad (3)$$

Using the vector model, we obtain the distribution $P(M_I,M_\gamma)$ of the magnetic substates M_I:

$$P(M_I,M_\gamma)=\left[C_1+C_2\exp\left[-\frac{(I-M_I)^2}{2\sigma_{M_I}^2}\right]\right]\Big/\sum\left[C_1+C_2\exp\left[-\frac{(I-M_I)^2}{2\sigma_{M_I}^2}\right]\right], \quad (4)$$

where $M_I=I\sin\beta$ and $\sigma_{M_I}=I\sin\sigma_\beta$. The values of the coefficients C_1, C_2, and σ_β were obtained from tabulated values corresponding to differenct γ-emission patterns of certain multiplicity and multipole mixing for the systems under study. In our calculations for the Yb* isotopes, typical values of the FWHM of the spin-alignment response function, Eq. (3), were 72°, 66°, 64°, 62°, and 60° for the multiplicity bins $M_\gamma=11-14$, 15–18, 19–22, 23–26, and 27–33, respectively. The corresponding values were increased by almost 2° in the case of ^{114}Sn*. The coefficients $B_\lambda(I_i)$ are given by[34]

$$B_\lambda(I_i)=\sum(-1)^{I_i-M_I}(2I_i+1)^{1/2}P(M_I,M_\gamma)\times\langle I_iI_i-M-M|\lambda 0\rangle. \quad (5)$$

In order to calculate the A_2 coefficients, the events from the previous statistical model calculations were sorted in bins 1 MeV wide in E_α and M_γ bins matching the experimental ones. For each α decay associated with a spin change $\Delta I=I_i-I_f$, the relative weights for each l value were obtained from the triangular condition $|\Delta I|\le l\le 2I_i-\Delta I$. The statistical sum of $a_{E_\alpha,I_i,I_f,2}B_2(I_i)$, associated with A_2, is compared to the experimental data below, for each M_γ bin as a function of E_α.

The results are compared to the experimental data for ^{114}Sn*, ^{138}Nd*, ^{164}Yb*, and ^{170}Yb* in Fig. 5. The pairs of curves are FWHM boundaries of the calculated A_2 coefficients. In the case of ^{114}Sn* [Fig. 5(b)], the trend as well as the absolute magnitude of the anisotropies is reproduced. For ^{138}Nd* [Fig. 5(c)], the trend and absolute magnitude of the A_2's is reproduced for the highest fold bin ($k_\gamma=27-33$). For the first three fold bins, the calculated coefficients have greater slopes than the data. No clear deviations between theory and experiment can be inferred, except for the possibility of a small downturn of the data in the $k_\gamma=27-33$ bin at very low energies. In the cases of ^{164}Yb* [Fig. 5(d)] and ^{170}Yb* [Fig. 5(e)], good agreement is obtained for most of the fold bins at energies above the Coulomb barrier ($\approx$20 MeV). There are clear deviations with the trend of the data at sub-barrier energies which increase with spin. As the energy decreases, the calculated coefficients suggest monotonically decreasing anisotropies, although their slopes slightly decrease. In some cases a downturn is predicted in the sub-barrier region.

The origin of the downturn of the calculated A_2 coefficients, in this case, is traced to α transitions originating from states close to the yrast line. There, the scarcity of states accessible for small ΔI promotes low-energy α emission with fairly large ΔI and l in spite of the small T_l values. The large contributing l values cause a decrease in the slope of the calculated A_2's, and, eventually, their downturn. This effect can be seen when the α-emitting states are examined on the excitation energy versus angular momentum plane. Such a representation is examined in the next section.

A calculation for the A_2 coefficients for ^{110}Sn*, using the parameters of the ^{114}Sn* case, was able to reproduce the experimental trend of the data but not their absolute magnitude. The experimental A_2 coefficients of ^{110}Sn* are smaller in absolute magnitude than those of the ^{114}Sn*. Since the γ-decay properties in the two Sn* cases are not expected to differ significantly, we attribute the attenuation to multiple α emission of the more neutron-deficient ^{110}Sn*.

The general features of this calculation are as follows. (a) There is agreement with the ^{114}Sn* data both in the 90° center of mass spectra and A_2 coefficients. (b) In the ^{138}Nd* and the Yb* cases, there is an underprediction of the sub-barrier spectra and deviations from the experimental A_2 coefficients, in the same energy region. These deviations become stronger from the ^{138}Nd* to ^{170}Yb*

and increase with angular momentum. Discrepancies of this type in the energy spectra have been attributed to a deformation effect by many authors.[8,9,13,35] The assumption of a deformed nucleus (with a lower evaporation barrier) can account both for the excess of the sub-barrier spectra and the downturn of the A_2 coefficients. Such an effect appears in the level densities and the transmission coefficients for charged-particle emission. Although our level density formalism is based on spherical nuclei, deformation effects were partially taken into account by the yrast lines used. Therefore, the most important element in the calculation responsible for the above discrepancies is the transmission coefficients.

Examining the sensitivity of the calculated quantities in statistical model parameter changes, we found a dependence of the sub-barrier anisotropies on the γ strengths $B(E1)$ and $B(E2)_{\text{coll}}$. Increasing these strengths has the effect of limiting the number of sub-barrier α transitions and reducing the downturn of the A_2 coefficients. The shape of the yrast line also plays an important role. A flatter yrast line has the same effect as increasing the γ strengths, besides affecting the high-energy slopes of the particle spectra. The opposite effect is seen when a steeper yrast line is used. The choice of the yrast lines and γ strengths was based on our experience from experimental results on our systems. Steeper but unrealistic yrast lines than the ones used tend to closely reproduce the behavior of the A_2 coefficients. However, they produce strong deviations from the measured xn and αxn cross sections for ^{170}Yb* and disallow such adjustments.

The attenuation of the A_2 coefficients introduced by the B_2's of Eq. (5) was estimated from the ratio of the calculated A_2 values to the ones assuming full alignment. This is best represented by a coefficient

$$\alpha_2 \equiv B_2(I)/B_2^{\max}(I) ,$$

which gives the attenuation of the theoretical maximum due to the response of the Spin Spectrometer. $B_2^{\max}(I)$ was calculated assuming a population of magnetic substates: $P(M)=\delta_{M,I}+\delta_{M,-I}$ and I was taken equal to the average spin $\langle I_i \rangle$ of the α-emitting states within the relevant M_γ gates. The resulting α_2 coefficients are given in Table III for ^{114}Sn* and ^{170}Yb* and correspond to the near barrier alpha-particle energies of 15 MeV and 20 MeV, respectively.

A comparison of the anisotropies with respect to the estimated spin direction with those that would be observed in a singles experiment with respect to the beam direction would be useful. Since in this work we did not obtain the latter distribution, an estimate was made as follows. The experimental distributions with respect to spin and the gating conditions of Table III were fitted with the semiclassical relation

$$W(\beta)=\exp(-B\cos^2\beta) ,$$

where B is a constant and β is the angle with respect to spin.[42] This fit produced the values denoted by B' in Table III. A second fit was made with this equation folded with the spin-alignment response function in an iterative procedure to yield the experimental ratios $R_S=W(90°)/W(0°)$. This procedure determined the unattenuated coefficients B. The integration about the beam axis results in an anisotropy[42]

$$R_B \equiv W(0°)/W(90°)=\exp(B/2)/I_0(B/2) ,$$

where I_0 is a Bessel function of the first kind of imaginary argument. The ratio of the experimental anisotropy R_S to R_B is given in the last row of Table III. We see that for both reaction systems, the anisotropy ratios with respect to the estimated spin direction are in general stronger than those with respect to the beam, except for the lowest γ-ray multiplicity bins.

TABLE III. Comparison of the angular correlation parameters with respect to the estimated spin and with respect to the beam direction.

			^{114}Sn*		
M_γ	11-14	15-18	19-22	23-26	27-33
$\langle I_i \rangle$	31	41	49	57	61
α_2	0.23	0.26	0.28	0.29	0.31
R_S	1.44	1.87	2.44	2.91	3.26
B'	0.35	0.59	0.84	0.99	1.09
B	1.02	1.59	2.24	2.62	2.87
R_B	1.56	1.90	2.29	2.51	2.65
R_S/R_B	0.92	0.98	1.07	1.16	1.23
			^{170}Yb*		
M_γ	11-14	15-18	19-22	23-26	27-33
$\langle I_i \rangle$	29	38	47	56	64
α_2	0.22	0.26	0.29	0.32	0.34
R_S	1.25	1.39	1.57	1.64	1.56
B'	0.25	0.35	0.46	0.50	0.45
B	0.53	0.72	0.93	0.94	0.52
R_B	1.28	1.39	1.51	1.52	1.27
R_S/R_B	0.97	1.00	1.04	1.08	1.23

D. A simulation of the deformation effects

A simulation of deformation effects in the statistical model formalism was performed in the case of the Yb* isotopes, in order to get an estimate of the effect in systems which show the largest deviations from the predictions of the model with standard parameters. For this purpose we employed a variation of the method of equivalent spheres,[8,36] which has been used successfully in the description of sub-barrier fusion data with statically deformed targets.

The daughter nucleus was assumed to have an axially symmetric prolate shape, which was parametrized in terms of the quadrupole deformation parameter β_2 as

$$R(\theta)=R_0[1+X(\beta_2)+\sqrt{5/4\pi}\beta_2 P_2(\cos\theta)] . \quad (6)$$

Here, θ is the angle with respect to the symmetry axis and $X(\beta_2)=-\beta_2^2/4\pi$ is the volume conservation term. Optical model transmission coefficients for protons and alphas were calculated for all of the nuclei in the cascade at nine different angles from 5° to 85° in steps of 10°. At each angle, the optical model radii were scaled according to Eq. (6). The diffuseness of the Woods-Saxon nuclear potential of the spheroid was also modified, so that the normal derivative at each point on an equipotential surface is unaffected by the deformation.[31] The above transmission coefficient sets were stored in computer files to be read by PACE2D. In the execution of the program, charged-particle emission from a particular point of the emitter nucleus surface was selected with a random number weighted by the corresponding surface element of the spheroid: $2\pi R^2(\theta)\sin\theta\Delta\theta/S$. Here, S is the nuclear surface including the first-order correction term due to deformation:

$$S=4\pi R_0^2(1+a_2^2/5) ,$$

with $a_2=\sqrt{5/4\pi}\beta_2$. A simulation that identifies the detection angle with the emission point of the decaying nucleus would be useful.[15] However, at the present stage of approximations we feel that the above procedure can closely describe the effect expected to be seen in the 90°

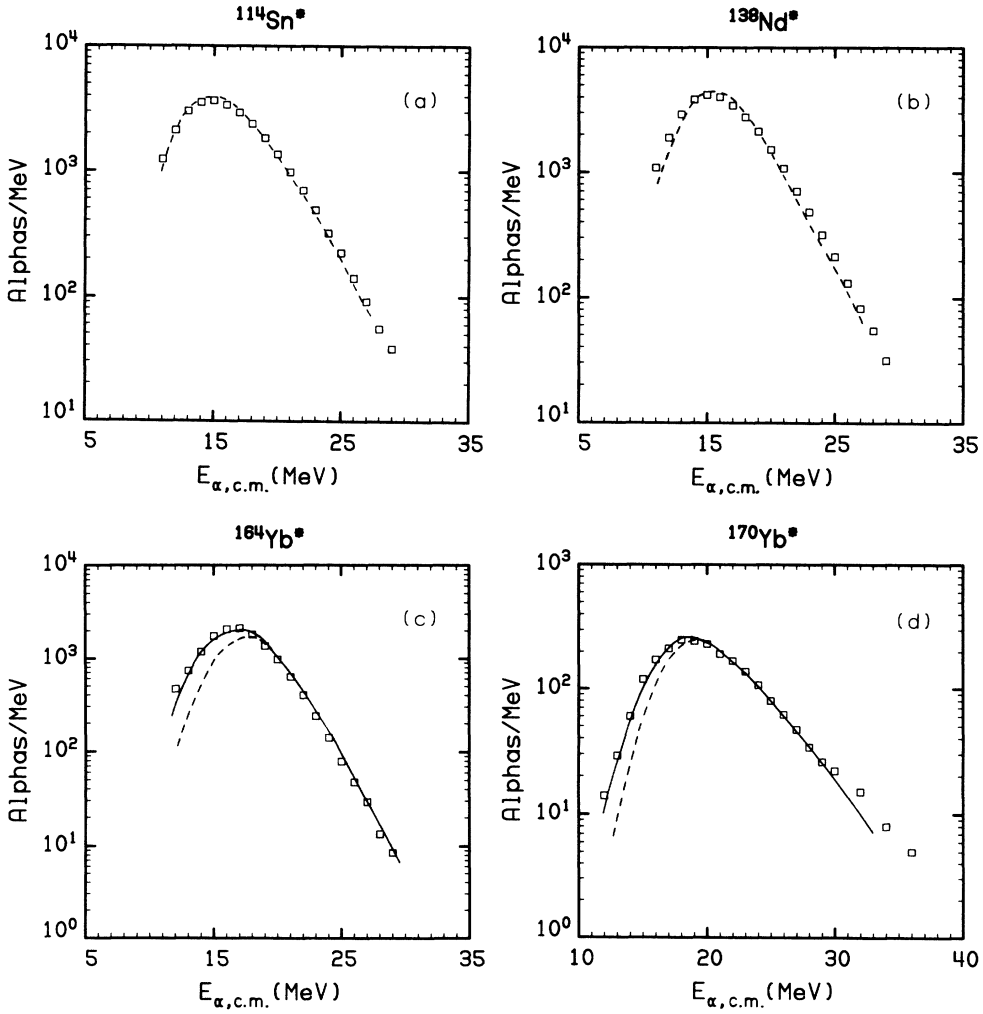

FIG. 6. Experimental 90° center of mass spectra integrated over k_γ (≥ 11) and β for (a) ^{114}Sn*, (b) ^{138}Nd*, (c) ^{164}Yb*, and (d) ^{164}Yb*. The solid and dashed lines represent the result of calculations discussed in the text.

center-of-mass spectra.

The results of this calculation for the 90° center of mass spectra of ^{164,170}Yb* is shown in Figs. 6(c) and (d) by the solid lines. A deformation of $\beta_2=0.2$ was assumed in both cases. For ^{164}Yb*, a slightly larger deformation is still needed. For ^{170}Yb*, a good description is obtained in the whole energy region. These calculations were performed with the parameters listed in Table II, except that the level density parameters were decreased to $a=A/9.5$ and $A/10.5$, respectively. This is a consequence of the limitations imposed by the scaling of Eq. (6) and the assumed weighting according to the corresponding surface element. For an emission along the major axis of the prolate spheroid (larger radius), we get an enhancement of the contributing partial waves for all of the energies, compared to the emission along the minor axis (smaller radius). The emission along the waist is weighted by a larger fraction of the nuclear surface. This limits the highest available partial waves at the highest energies and leads to softer spectra. The above change in the level density parameter was then necessary to compensate for this effect.

Such calculations can be used to demonstrate the angular momentum dependence of the deformation effect. We saw in Fig. 2(c) that for ^{170}Yb*, the sub-barrier alpha yields of the 90° center of mass spectra are underpredicted by the statistical model calculation assuming transmission coefficients derived from a spherically symmetric potential. This calculation, represented by the dashed lines, shows that the underprediction of the sub-barrier yields increases with angular momentum. On the same plot, the solid line for the $k_\gamma=11-14$ bin shows the calculated spectrum with $\beta_2=0.2$. The sub-barrier data points lie between the curves $\beta_2=0$ and $\beta_2=0.2$. In this case, a deformation smaller than $\beta_2=0.2$ is required to fit the spectrum. On the other hand, for the high-spin case $k_\gamma=27-33$, $\beta_2=0.2$ was insufficient to account for the excess of sub-barrier alphas. The dashed curve in the figure corresponds to $\beta_2=0.35$ and fits the spectrum closely. These calculations show us the extent of the angular momentum dependence of the effect. The originally deduced $\beta_2=0.2$ was based on the total 90° center of mass spectrum and represents an average over different deformed shapes.

Emissions from the tip of the spheroid favor the sub-barrier alphas and involve large-l partial waves which lead to strong anisotropies [Eq. (2)]. According to the arguments of the preceding section, such transitions are expected to take place from low excitation states, close to the yrast line. This effect can be examined when the α-emitting states are plotted on the excitation energy (E^*) vs angular momentum (I) plane. Using the information of the event files from PACE2D, decay maps of the α-emitting states were constructed for all of the systems under study. We present the results of such a representation from the deformed calculation for ^{170}Yb* with a deformation parameter of $\beta_2=0.2$. In Figs. 7(a)–(c), we show on the E^* vs I plane the population of α-emitting states in the reaction ^{20}Ne+^{150}Nd→^{170}Yb*. The maps include α transitions of any chance subjected to the gating conditions described below. For reference, the ^{166}Er yrast line is shown on the figure by the solid line. It is to be understood that for different decay chains, different yrast lines are important, depending on the nature and the number of the emitted particles. The map in Fig. 7(a) shows the α-emitting states throughout the whole deexcitation process. The corresponding emitted alpha particles form the calculated spectrum of Fig. 6(d), in the energy range $E_\alpha=10-30$ MeV. By setting E_α gates in the sorted events, interesting features appear. Figures 7(b) and (c) show the (E^*,I) maps corresponding to the E_α

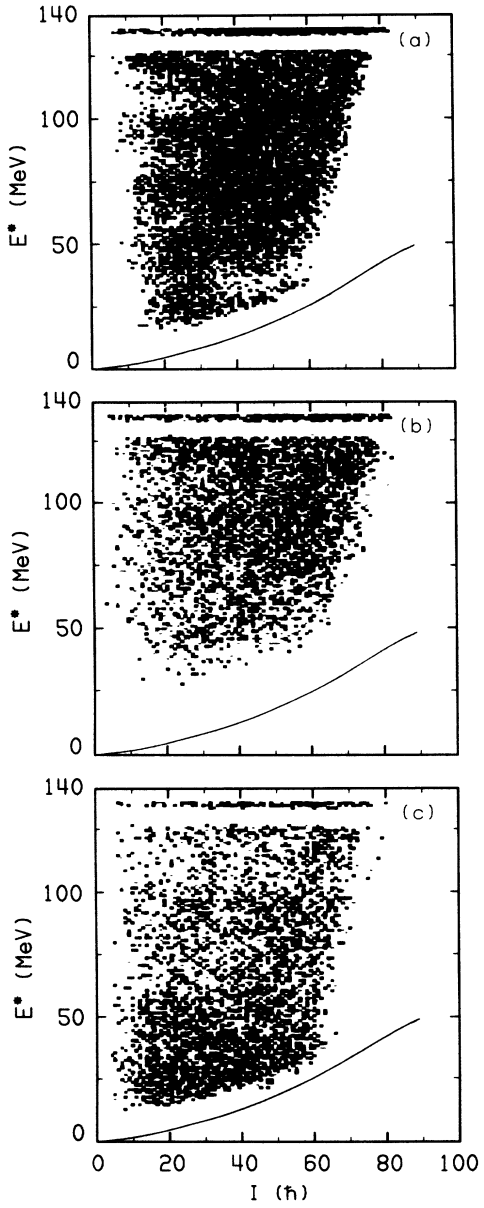

FIG. 7. Excitation energy versus angular momentum plots of the α-emitting states of ^{170}Yb*, deduced from the statistical model calculation with PACE2D. In (a) all of the α-emitting states with $E_\alpha=10-30$ MeV have been included. The maps (b) and (c) show the E_α-gated events with $E_\alpha=22-24$ MeV and $E_\alpha=14-16$ MeV, respectively. In all of the cases the ^{166}Er* yrast line is shown for reference.

gates 22–24 MeV and 14–16 MeV, respectively. In the map corresponding to the high E_α gate [Fig. 7(b)], the population of the α-emitting states at some excitation energy E^* increases with I, and all of these states are remote from the yrast lines. In the case of the sub-barrier gate [Fig. 7(c)], although there are emitting states on the whole (E^*,I) plane, there is a small excess of such states close to the yrast line. This excess is limited in a range of $E^* \approx 25$ MeV above the yrast line. The same localization has been seen in the other sub-barrier maps of ^{170}Yb*.

Alpha particles emitted from these near-yrast states have to remove large amounts of angular momentum, due to the flatness of the yrast lines. Therefore, they introduce large anisotropies [Eq. (7)]. This effect can cause a downturn in the calculated A_2 coefficients at sub-barrier energies in the ^{164}Yb* and ^{170}Yb* isotopes. In the other systems, this effect is not very strong. It is completely absent in the lowest mass systems we studied. Although their (E^*,I) maps show an increasing population of α-emitting states at high angular momentum, their sub-barrier α transitions do not involve large angular momentum removals since their yrast lines are steeper.

It has to be noted that the above deformation calculation is based on an approximate model. It merely shows that such a simulation points in the right direction for the purpose of explaining the alpha-particle spectra. There are different sources of uncertainty in the deduced magnitude of the effect. (a) In the optical model calculations, lower-order effects like the quadrupole interaction and changes in the curvatures of the surfaces at the point of contact were neglected. (b) The transmission coefficients at a given angle with respect to the symmetry axis were calculated within the sudden approximation.[36] In our case, this approximation is expected to be adequate. Since the moment of inertia of the emitting system is large, no significant rotation may occur during its interaction with an alpha particle. (c) A "unique" treatment for all of the nuclei in the cascade has been made as far as deformation and emission angle is concerned. A constant deformation was assumed, although the deexciting nuclei may assume a variety of shapes, depending on their intrinsic excitation and spin. However, the final result for the alpha spectra was produced after an averaging over all of the emission angles, taking into account the proper weighting factor.

The assumption of a particular shape of the α-emitting nucleus plays a restrictive role in the magnitude of the deduced deformation. For a prolate emission shape, the sub-barrier enhancement is affected by two opposing factors: (a) the effective barrier modulation, at a given angle, which favors emissions along the major axis of the spheroid [Eq. (6)], and (b) the statistical weight of the different orientations which favors emissions along the minor axis. In the case of an oblate shape, these factors increase in the same direction and favor emissions along the major axis. However, such a geometry would require a slightly larger deformation to produce the reduction in the evaporation barrier needed to reproduce the data. This can be understood in terms of the scaling of Eq. (6), which predicts a greater maximum radius for a prolate than an oblate shape of the same deformation (see also Ref. 36).

The calculated A_2 coefficients show a trend approaching the experimental data at sub-barrier energies. However, no quantitative statement can be made from such comparisons, because our formalism [Eqs. (1) and (2)] is limited to spherically symmetric emitters. More refined calculations are required for this purpose. Work in this direction is in progress.[40,41]

In the above calculations, the effect of nuclear deformation was studied in the transmission properties of the emitting system. The nuclear deformation also enters in the level density expression through the yrast line. The yrast lines we used were constrained by the experimental values which are known up to very high spin. The rare-earth systems exhibit deformations[30] whose effects are included in the yrast lines. In this sense, our spherically symmetric calculation actually involves some elements of deformation. However, our statistical model code employs level density expressions appropriate for spherical nuclei. A consistent simulation of deformation effects should also include the effect of collective enhancements in the level densities. Although this subject deserves further investigation, we believe that such modifications affect mainly the high-energy α emission, where the major role is played by the level densities.

E. Discussion

In the preceding sections, our experimental data were compared with two different kinds of statistical model calculations. The first one was identified as "spherically symmetric" and provided a good description of both the 90° center of mass spectra for ^{110,114}Sn* and the trend of the A_2 coefficients for ^{114}Sn*. With the same optical model parameter set and reasonable choices of the statistical model parameters, we observe discrepancies in the corresponding observables for the other systems. The discrepancies become larger for the heaviest systems under study, namely the decay of the Yb* isotopes. They consist of an underprediction of the sub-barrier spectra and deviations in the anisotropy coefficients which increase with spin.

One might question how reasonable the optical model parameters are for describing the α emission behavior of a spherical system in the mass ≈ 170 region. We have tested how well the inverse cross sections we used describe fusion data for alpha particles with targets close to our compound nuclei.[39] The data of Broda *et al.*,[37] concerning the fusion of alpha particles with ^{162}Dy, were used for this purpose. The fusion cross section data are compared to the results of our optical model calculation, as a function of the alpha-particle energy in the laboratory system, in Table IV. In general, we have a reasonably good agreement for $E_\alpha \geq 19$ MeV, although the 17 MeV point is overestimated by almost a factor of 2. The lack of a sufficient number of sub-barrier data prevents us from making a detailed test of our calculation. Strictly speaking, even a calculation which exactly reproduces the above excitation function cannot qualify as a "spherically symmetric" one, because ^{162}Dy possesses a static deformation in its ground state. Therefore, our calculation

TABLE IV. Experimental (Ref. 37) and calculated cross section for the fusion of $\alpha + {}^{162}$Dy.

E_α (MeV)	σ_f (mb)	σ_{calc} (mb)
17.0	25.0±4.0	59.0
19.0	250.0±21.0	253.1
21.0	526.0±21.0	508.9
23.0	760.0±23.0	740.5
24.0	851.0±22.0	824.4
25.0	943.0±26.0	935.7
26.0	1039.0±26.0	1021.3
27.0	1115.0±27.0	1099.9

represents a situation *approaching* the spherically symmetric case.

On the basis of the discrepancies found in the sub-barrier Yb* spectra alone, several authors have discussed deformation effects in the compound nucleus decay.[8,9,35] Our data provide evidence of an angular-momentum-induced effect which appears not only in the alpha spectra, but in the anisotropy coefficients of the α emission with respect to the estimated spin direction as well. Our simple simulation for emission from a deformed system accounts successfully for the sub-barrier discrepancies of the alpha spectra, with an assumed average deformation of $\beta_2 = 0.2$ in the Yb* decays. For ^{170}Yb*, the comparison with the multiplicity-gated spectra revealed a magnitude of deformation less than 0.2 in the $k_\gamma = 11-14$ bin which increases to $\beta_2 = 0.35$ in the $k_\gamma = 27-33$ bin. The corresponding spins of the α-emitting states in the two cases are $\approx 34\hbar$ and $64\hbar$, respectively. The rotating liquid-drop model[3] predicts for ^{170}Yb* an elongated triaxial shape with an axis ratio of ≈ 1.2 (or $\beta_2 \approx 0.2$) at spin $60\hbar$. We can interpret the required excess of deformation as being caused by a polarization of the Coulomb barrier profile of the emitting system. A deformation effect of a smaller magnitude is suggested in the ^{138}Nd* decay, although the comparison between the experimental and theoretical A_2 coefficients is, in this case, inconclusive. Finally, no evidence for modifying the transmission coefficients in the Sn* cases was found. However, it has to be remembered that part of the deformation effects is "hidden" in the experimental yrast lines we used in the study of the above systems. Our analysis shows a sensitivity of the rare-earth region systems in deformation effects related to transmission over the mass ≈ 100 systems.

The implied differences in the shapes of the Yb* and Sn* compound nuclei may be compared with the observation of the decay of giant resonances built on excited states of similar compound nuclear systems. Giant resonance data from the decay of ^{166}Er* (61.5 MeV) suggest a two-component resonance in contrast to the decay of ^{108}Sn* (61.2 MeV), where a single resonance peak was observed.[6] In the first case, the fitted GDR strength ratios favor prolate shapes corresponding to a nuclear deformation of $\beta_2 \approx 0.28$. In the second, the observed strength function suggests that on the average, the nuclei retain their spherical shape, although different oblate shapes are probably induced at high spin and temperature.[7]

However, direct comparisons between the two methods are difficult to make since the two methods employ different probes and are sensitive to different regions of the (E^*, I) plane. The GDR method studies the ensemble of the γ-emitting nuclei, while the alpha-particle method studies the critical α-decay shapes. Just as important is the difference in the regions of the (E^*, I) space probed by these techniques. Alpha-particle competition becomes stronger at a given excitation energy as the yrast line is approached (stretched transitions). An $E1$ photon populating the same final state (same final level density) must originate from a state with greater thermal energy. Therefore, in a heavy-ion reaction, the alpha-particle technique is sensitive to a broader range of excitations on the (E^*, I) plane than the GDR technique.

There are fundamental questions concerning the origin of the lowering of the evaporation Coulomb barrier. One possibility originates from the fact that in a state of rapid rotation, the emitting system may attain a deformed shape. Its lower Coulomb barrier then causes an enhancement of the α-decay mode which is noticeable in the sub-barrier spectra. On the other hand, it has been pointed out that alpha-particle emission might cause a shape polarization of the two fragments such that the distance between the centroids of the two charge distributions exceeds that of two touching spheres.[38] Both of the above pictures are consistent with a lowering of the evaporation Coulomb barrier. Furthermore, a difference in the α-decay patterns from different emission shapes has not been confirmed. The α-decay patterns sample a large number of different decay chains in which the deexciting nuclei can be found in a variety of conditions and therefore nuclear shapes. The deviations we have observed in the Yb* isotopes indicate an average discrepancy from the behavior of a spherical system.

Our results on the α-emitting states from a deformed system show a concentration of the deformed α-emitting states close to the yrast line. Theoretical predictions support the existence of deformed nuclear shapes under similar conditions. Such effects have to be examined experimentally in properly designed experiments of alpha-particle counting in coincidence with yrast γ transitions.

V. CONCLUSIONS

The study of deformation effects in the compound nucleus decay through its charged-particle emission properties is a difficult but challenging project of the current heavy-ion research. The difficulties arise from the complexity of the deexcitation process and the proper interpretation of the experimental results.

The development of the spin-alignment method with the Spin Spectrometer has given us the ability to study in detail the important correlation of the alpha-particle emission with respect to the estimated spin direction. The study of α-γ correlations in the five compound nuclear systems we have examined has revealed differences in their decay patterns. The trend of the anisotropy coefficients of the closed proton shell Sn* compound nuclei suggests a nearly spherical emitting system. It is well described by a statistical model calculation assuming

standard optical model parameters for α emission. However, the experimental sub-barrier anisotropies of the Yb* isotopes deviate strongly from this trend, in a manner that increases with spin. At the same time, the sub-barrier α spectra are underestimated by the calculation. A deformation effect of the emitting system has been proposed as the cause of the above deviations. Our findings resemble the results of studies of giant resonances built on excited states of similar compound nuclear systems.

Inclusion of deformation effects in the statistical model has provided a description of the alpha-particle spectra of the decay of the Yb* isotopes. The deduced deformation, with a simplified model, is comparable in magnitude to the one deduced from giant resonance studies. However, a quantitative comparison of the two methods does not seem possible due to differences associated with the nature of the two probes. The simulation of deformation effects has shown that the extra alphas needed to fit the particle spectra originate from low excitation energy states, close to the yrast line. This can be used as a starting point for new experimental investigations.

ACKNOWLEDGMENTS

This work was supported in part by the U.S. Department of Energy under Contract No. DE-FG02-88ER40406. Support from the Robert A. Welch Foundation is also gratefully acknowledged.

*Present address: Medical Department, Brookhaven National Laboratory, Upton, NY 11973.

†Deceased, March, 1987.

‡On leave from the Institute of Physics, Jagellonian University, PL-30059, Krakow, Poland.

§Present address: Physics Department, Institute of Atomic Energy, Beijing, People's Republic of China.

**Present address: Wadsworth Center for Laboratories and Research, New York State Department of Health, Albany, NY 12201.

††Present address: INFN, Sezione di Padova, I-35131 Padova, Italy.

[1]P. J. Nolan and P. J. Twin, Annu. Rev. Nucl. Part. Sci. **38**, 533 (1988).

[2]J. Dudek and W. Nazarewicz, Phys. Rev. C **31**, 298 (1985); J. Dudek, T. Werner, and L. L. Riedinger, Phys. Lett. B **211**, 252 (1988).

[3]S. Cohen, F. Plasil, and W. Swiatecki, Ann. Phys. (N.Y.) **82**, 557 (1974).

[4]A. L. Goodman, Nucl. Phys. **A352**, 30 (1981).

[5]A. L. Goodman, Phys. Rev. C **37**, 2162 (1988).

[6]J. J. Gaardhøje, C. Ellegaard, and B. Herskind, Phys. Rev. Lett. **53**, 148 (1984).

[7]R. D. Chakrabarty, S. Sen, M. Thoennessen, N. Alamanos, P. Paul, R. Schicker, J. Stachel, and J. J. Gaardhøje, Phys. Rev. C **36**, 1886 (1987).

[8]M. Blann and T. T. Komoto, Phys. Scr. **24**, 93 (1981).

[9]J. M. Alexander, D. Guerreau, and L. C. Vaz, Z. Phys. A **305**, 313 (1982).

[10]F. A. Dilmanian, D. G. Sarantites, M. Jääskeläinen, H. Puchta, R. Woodward, J. R. Beene, D. C. Hensley, M. L. Halbert, R. Novotny, L. Adler, R. K. Choudhury, M. N. Namboodiri, R. P. Schmitt, and J. B. Natowitz, Phys. Rev. Lett. **49**, 1909 (1982).

[11]Z. Majka, D. G. Sarantites, L. G. Sobotka, K. J. Honkanen, E. L. Dines, L. A. Adler, Ze Li, M. L. Halbert, J. R. Beene, D. C. Hensley, R. P. Schmitt, and G. Nebbia, Phys. Rev. Lett. **58**, 322 (1987).

[12]N. G. Nicolis, D. G. Sarantites, L. A. Adler, F. A. Dilmanian, K. J. Honkanen, Z. Majka, L. G. Sobotka, Z. Li, T. M. Semkow, J. R. Beene, M. L. Halbert, D. C. Hensley, J. B. Natowitz, R. P. Schmitt, D. Fabris, G. Nebbia, and G. Mouchaty, Bull. Am. Phys. Soc. **32**, 1077 (1987); N. G. Nicolis *et al.*, in *The Variety of Nuclear Shapes,* edited by J. D. Garrett, C. A. Kalfas, G. Anagnostatos, and R. Vlastou (World Scientific, Singapore, 1987), pp. 526–536.

[13]Z. Majka, M. E. Brandan, D. Fabris, K. Hagel, A. Menchaca-Rocha, J. B. Natowitz, G. Nebbia, G. Prete, B. Sterling, and G. Viesti, Phys. Rev. C **35**, 2125 (1987).

[14]T. D. Thomas, Annu. Rev. Nucl. Sci. **18**, 343 (1968).

[15]N. N. Ajitanand, G. LaRana, R. Lacey, D. J. Moses, L. C. Vaz, G. F. Peaslee, D. M. de Castro Rizzo, M. Kaplan, and J. M. Alexander, Phys. Rev. C **34**, 877 (1986).

[16]L. C. Vaz and J. M. Alexander, Z. Phys. A **318**, 231 (1984).

[17]T. Ericson, Adv. Phys. **9**, 425 (1960).

[18]D. G. Sarantites, R. Lovett, and R. Woodward, Nucl. Instrum. Methods **171**, 503 (1980).

[19]M. Jääskeläinen, D. G. Sarantites, R. Woodward, F. A. Dilmanian, J. T. Hood, R. Jääskeläinen, D. C. Hensley, M. L. Halbert, and J. H. Barker, Nucl. Instrum. Methods **204**, 385 (1982).

[20]K. J. Honkanen, F. A. Dilmanian, D. G. Sarantites, and S. P. Sorensen, Nucl. Instrum. Methods **257**, 233 (1987).

[21]D. G. Sarantites, F. A. Dilmanian, M. Jääskeläinen, H. Puchta, R. Woodward, J. R. Beene, J. H. Barker, M. L. Halbert, J. Hattula, D. C. Hensley, I. Y. Lee, W. T. Milner, F. Plasil, J. J. Gaardhoje, J. D. Garrett, G. B. Hagemann, B. Herskind, P. Nolan, and G. Sletten, in *High Angular Momentum Properties of Nuclei,* edited by N. R. Johnson (Harwood, Academic, Chur, Switzerland, 1983), pp. 417–435.

[22]A. Gavron, Phys. Rev. C **21**, 230 (1980); modification PACE2S by J. R. Beene.

[23]D. Wilmore and P. E. Hodgson, Nucl. Phys. **55**, 673 (1964).

[24]C. M. Perey and F. G. Perey, Nucl. Data Tables **17**, 1 (1976).

[25]L. McFadden and G. R. Satchler, Nucl. Phys. **84**, 177 (1966).

[26]G. R. Satchler, Nucl. Phys. **70**, 177 (1965).

[27]R. Bass, Phys. Rev. Lett. **39**, 265 (1977).

[28]M. L. Halbert, R. A. Dayras, R. L. Ferguson, F. Plasil, and D. G. Sarantites, Phys. Rev. C **17**, 155 (1978).

[29]A. J. Sierk, Phys. Rev. C **33**, 2039 (1986).

[30]M. J. A. de Voigt, J. Dudek, and Z. Szymanski, Rev. Mod. Phys. **55**, 949 (1983).

[31]A. Bohr and B. R. Mottelson, *Nuclear Structure* (Benjamin, Reading, MA, 1975), Vol. II.

[32]S. S. Hanna, in *Giant Multipole Resonances,* edited by F. Bertrand (Harwood, New York, 1980), Table I.

[33]D. G. Sarantites, J. H. Barker, M. L Halbert, D. C. Hensley, R. A. Dayras, E. Eichler, N. R. Johnson, and S. A. Gronemeyer, Phys. Rev. C **14**, 2138 (1976).

[34]M. E. Rose, *Elementary Theory of Angular Momentum* (Wi-

ley, New York, 1957).
[35]M. A. McMahan and J. M. Alexander, Phys. Rev. C **21**, 1261 (1980).
[36]D. E. Di Gregorio, J. O. Fernandez Niello, A. J. Pacheco, D. Abriola, S. Gil, A. O. Macchiavelli, J. E. Testoni, P. R. Pascholati, V. R. Vavin, R. Liguori Neto, N. Carlin Filho, M. M. Coimbra, P. R. Silveira Gomes, and R. G. Stokstad, Phys. Lett. B **176**, 322 (1986). See also R. G. Stokstad and E. E. Gross, Phys. Rev. C **23**, 281 (1981), and references therein.
[37]R. Broda, M. Ishihara, B. Herskind, H. Oeschler, S. Ogaza, and H. Ryde, Nucl. Phys. **A248**, 356 (1975).
[38]L. G. Moretto, Nucl. Phys. **A247**, 211 (1975).
[39]L. C. Vaz and J. M. Alexander, in *Fusion Reactions Below the Coulomb Barrier* (Springer-Verlag, Berlin, 1984), p. 288.
[40]T. Berggren and P. Olanders, Report Lund-Mph-87/05, 1987.
[41]V. P. Aleshin (unpublished).
[42]L. C. Vaz, J. M. Alexander, and N. Carjan, Z. Phys. A **324**, 331 (1986).
[43]R. Lacey, N. N. Ajitanand, J. M. Alexander, D. M. de Castro Rizzo, G. F. Peaslee, L. C. Vaz, M. Kaplan, M. Kildir, G. La Rana, D. J. Moses, W. E. Parker, D. Logan, M. S. Zisman, P. DeYoung, and L. Kowalski, Phys. Rev. C **37**, 2561 (1988).